ADVANCES IN ATMOSPHERIC SCIENCES, VOL. 41, DECEMBER 2024, 2432–2445

• **Original Paper** •

Characteristics and Formation Mechanisms of Low-Level Jets in Northeastern China

Hailong SHU[1], Fan ZHANG[*2], Yu DU[*3], Yue WANG[1], Huichuang GUO[1], Zhen SONG[1], and Qinghong ZHANG[4]

[1]*State Key Laboratory of NBC Protection for Civilian*, *Beijing* 102205, *China*

[2]*State Key Laboratory of Severe Weather*, *Chinese Academy of Meteorological Sciences*, *Beijing* 100081, *China*

[3]*School of Atmospheric Sciences*, *Sun Yat-Sen University*, *and Southern Marine Science and Engineering Guangdong Laboratory (Zhuhai)*, *Zhuhai* 519082, *China*

[4]*Department of Atmospheric and Oceanic Sciences*, *School of Physics*, *Peking University*, *Beijing* 100871, *China*

(Received 14 November 2023; revised 27 May 2024; accepted 3 June 2024)

ABSTRACT

This study examines low-level jets (LLJs) across Northeastern China during both warm (June–September) and cold seasons (December–March) from 1957 to 2021, using fifth generation of the European Centre for Medium-Range Weather Forecasts reanalysis data with 25-km resolution. LLJs manifest in two prominent regions, one along the leeward flank of the Da Hinggan Ling Mountains in the cold season and another at the center of Northeastern China in the warm season. The intricate interplay between ambient circulation and terrain shapes LLJ distribution, altitudes, wind directions, diurnal cycles, and seasonal diversities. During the warm season, prevailing southwesterly LLJs are found at 925 hPa, while the cold season features stronger and more frequent northwesterly LLJs at 875 hPa. Analysis of the diurnal patterns reveals distinctive behaviors of LLJs in the cold and warm seasons. During the warm season, the single peak in LLJ occurrence emerges around midnight; conversely, in the cold season, LLJs are most frequent shortly before midnight, with an additional sub-peak in the morning. A momentum budget analysis establishes mechanisms underlying these two distinct diurnal variations. In both seasons, the diurnal variation of LLJs is predominately driven by an inertial oscillation and mountain-valley circulations. However, the sub-peak observed in the cold-season morning arises from the thermodynamic and dynamic interaction between the low-level atmosphere and complex terrain.

Key words: low-level jet, seasonal disparities, diurnal variation, inertial oscillation, terrain-flow interaction

Citation: Shu, H. L., F. Zhang, Y. Du, Y. Wang, H. C. Guo, Z. Song, and Q. H. Zhang, 2024: Characteristics and formation mechanisms of low-level jets in Northeastern China. *Adv. Atmos. Sci.*, **41**(12), 2432–2445, https://doi.org/10.1007/s00376-024-3209-8.

Article Highlights:

- Cold and warm seasons in Northeastern China exhibit spatially distinct high-frequency LLJ regions.
- The complex terrain and circulation in the Northeast contribute to the spatiotemporal distribution traits of LLJs.
- Diurnal variations of LLJs are primarily governed by inertial oscillations and display pronounced seasonal disparities.

1. Introduction

Low-level jets (LLJs) are significant meteorological phenomena that exert a vital influence across global regions. They can modulate water vapor transport and convergence, thereby affecting the local water vapor balance (Blackadar, 1957; Hoecker, 1963; Holton, 1967; Hsueh, 1970; Du et al., 2015a; Du and Chen, 2019; Luo and Du, 2023). Characterized by vertical wind shear, LLJs contribute to atmospheric instability and are favorable for the development and maintenance of convective activities (Maddox, 1983; Fritsch et al., 1986). Additionally, LLJs bear important implications for wind energy, flight safety, and air quality (Liu et al., 2014), rendering their investigation pivotal within meteorology.

Considerable efforts have been made toward exploring the mechanisms of LLJs from diverse perspectives. According to the theory by Blackadar (1957), inertial oscillations constitute a key factor in LLJ formation. These oscillations of the ageostrophic winds result from sudden eddy viscosity decay after sunset, leading to clockwise rotation of the ageostrophic wind component and the subsequent emergence

* Corresponding authors: Fan ZHANG, Yu DU
Emails: zhang_fan@cma.gov.cn, duyu7@mail.sysu.edu.cn

of LLJs as a byproduct of super-geostrophic winds. Holton (1967) emphasizes the role of thermal contrast between the mountains and plains in LLJ formation. Such a contrast arises from imbalanced solar radiation heating, engendering diurnal oscillations in the boundary layer wind above sloping terrains. Besides, terrain-induced blocking and channeling effects substantially contribute (Liu et al., 2014) and are prominently notable in regions like the eastern side of the Rocky Mountains (Wexler, 1961), the northern Bohai Sea (Zhang et al., 2018), and the southeastern coast of China (Li and Chen, 1998; Kong et al., 2020), where terrain significantly shapes low-level wind patterns. Liu et al. (2023) further highlight that different combinations of synoptic-scale disturbances and diurnal thermal forcing account for the diversity in LLJ formation. In essence, the formation of LLJs is a complex process orchestrated by multifaceted factors, often involving simultaneous or additive operation of multiple theories (Liu et al., 2014; Du and Rotunno 2014; Du et al., 2015b).

LLJs experience seasonal and diurnal variations in various regions. Numerous studies have examined these variations across the globe. In the United States, Whiteman et al. (1997) developed a climatology of the Great Plains LLJ using two years of research rawinsonde data from north-central Oklahoma. They noted the presence of an LLJ in 47% of warm-season and 45% of cold-season soundings, indicating seasonal discrepancies. Bonner (1968) analyzed two years of wind data from 47 rawinsonde stations and found that LLJs predominantly occurred with southerly flow, with southerly wind maxima being more frequent during morning observations. Song et al. (2005) utilized mini-sodars and 915-MHz wind profilers to scrutinize nocturnal LLJs at the Atmospheric Boundary Layer Experiments (ABLE) facility in Kansas. They found LLJs during 63% of the sampled nighttime periods, highlighting diurnal variations.

In China, Du et al. (2012) focused on Shanghai, developing an LLJ climatology during mei-yu and non-meiyu periods using wind profiler radar data. They revealed distinct diurnal cycles, with LLJ peaks during nighttime and early morning. Wang et al. (2013) and Wei et al. (2014) conducted comprehensive studies along the East China coast using multiple wind-profile radars to investigate LLJs. They revealed that LLJs displayed distinctive daily and seasonal structures with their dominant wind directions varying across seasons, which were observed to be southerly-southwesterly during spring and summer and northeasterly during autumn and winter, thus enhancing the comprehension of LLJ dynamics in response to seasonal shifts in East China.

Diverse data sources contribute to LLJ analysis. Direct observations offer high temporal and vertical resolutions, albeit at a single-point detection limitation. Radar networks and encrypted sounding observations enhance horizontal resolution, but cost considerations restrict the observation range. Numerical simulations have the advantage of high spatial and temporal resolutions, providing valuable LLJ insights in various regions (Du et al., 2015a; Zhang et al., 2018; Kong et al., 2020). Du et al. (2014) and Jiménez-Siménez et al. (2020) used hourly Weather Research and Forecasting (WRF) model output with a 9-km resolution to document LLJs over China and Orinoco River Basin, respectively. However, computational demands limit the time range of numerical simulations.

Reanalysis data strikes a balance, offering sufficient temporal and spatial resolution and an extended time range, suiting long-term research; notable studies exemplify its value. Rife et al. (2010) used the MM5-based version of the Climate Four-Dimensional Data Assimilation system to examine the global distribution of nocturnal LLJs; Wang et al. (2013) and Liu et al. (2014) delved into LLJs over southeastern China using the National Centers for Environmental Prediction (NCEP) Final (FNL) data; Lima et al. (2018) conducted a thorough investigation into global coastal low-level wind jets by employing an ensemble of reanalyses including ERA-Interim, JRA-55, and MERRA-2 to study; Ferguson (2022) and Du et al. (2022) employed ERA5 data to study LLJs in the Great Plains in the United States and South China, respectively.

The northeastern region of China, situated within the middle and high latitudes of East Asia, experiences complex circulation patterns. Warm seasons are characterized by southerly winds, while cold seasons feature prevailing northwesterly winds. The geography of Northeastern China is surrounded by four mountain ranges: the Da Hinggan Ling Mountains to the west, the Changbai Mountains to the east, the Xiao Hinggan Ling Mountains to the north, and the Yanshan Mountains to the south (Fig. 1). Socioeconomically, the Northeast China Plain is recognized as one of the world's four major black soil areas. The fertility of its soil makes the Northeast China Plain the most significant grain-producing area in China. Consequently, studies conducted within this region hold significant potential for deepening our understanding of the intricate interplay between circulation, topography, and meteorological phenomena, with far-reaching implications for food security.

Du et al. (2014) identified Northeastern China as one of the LLJ-active regions in China during the early summer months (May–July). Intriguingly, these LLJs frequently coincide with elevated terrain and exhibit considerable diurnal variations, suggesting a complex interaction between LLJ dynamics and the regional topographical features. However, our understanding of LLJs within this region remains incomplete, particularly during the cold season, where previous studies are notably lacking. Moreover, the thermodynamic and dynamic mechanisms underpinning the formation and variability of LLJs in both warm and cold seasons are not fully understood. These constitute the two primary scientific problems our paper aims to address.

To address the above-mentioned questions, we employ reanalysis data from ERA5 spanning the years 1957 to 2021, with the goal of dissecting the occurrences, spatiotemporal distributions, and diurnal variations of LLJs in Northeastern China during both warm and cold seasons. The

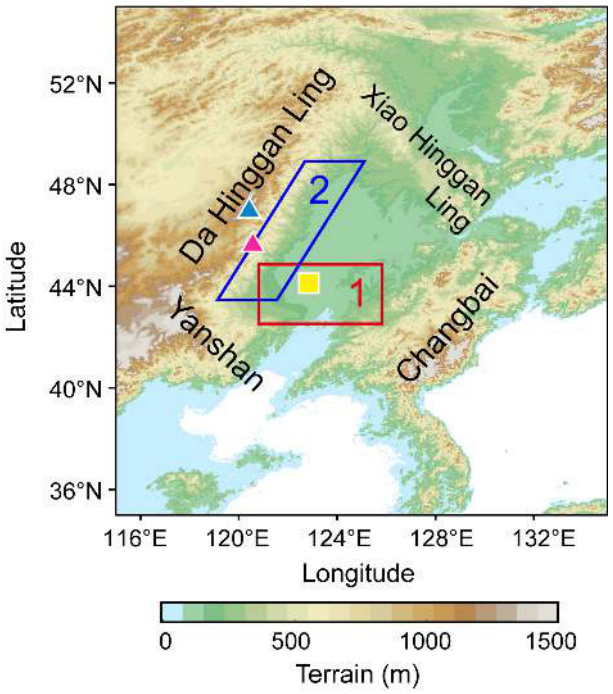

Fig. 1. The distribution of topography (m, shading) in Northeastern China with the names of major landforms labeled in text. The red (blue) box represents the high-frequency LLJ region in the warm (cold) season. The two triangles represent the peak and the eastern slope of the Da Hinggan Ling Moutains, while the square represents the foothills.

remainder of this paper is organized as follows. The methodology and data framework are described in section 2. In section 3, an in-depth analysis is conducted on the temporal and spatial distributions of LLJs over Northeastern China. Section 4 sheds light on the intricate mechanisms underpinning LLJ formation and development. Finally, a summary is provided in section 5.

2. Data and methodology

2.1. *Data*

The data utilized in this study is the hourly ERA5 reanalysis data provided by the fifth generation ECMWF reanalysis for the global climate and weather. The data has a temporal coverage from 1957, with a preliminary back extension covering 1957–78 and a final release plus timely updates covering 1979 onwards. The ERA5 reanalysis data boasts a fine horizontal resolution of 0.25 degrees and a comprehensive vertical profile, with 37 pressure levels ranging from 1000 to 1 hPa. This dataset is comprehensive enough to encompass the entire Northeastern China region, from 35° to 55°N and from 115° to 135°E (Fig. 1) covering the warm season (June–September) and cold season (December–March) over the period 1957–2021.

2.2. *Criteria for identifying LLJs*

In this study, we employed a definition of LLJs consistent with previous studies (Bonner, 1968; Muñoz et al., 2008; Rife et al., 2010). The definition of an LLJ was established by the following criteria: (1) a minimum wind speed of not less than 10 m s^{-1} below a pressure level of 600 hPa and (2) a decrease in wind speed of at least 5 m s^{-1} per 1000 m from the level of maximum wind speed to the level of minimum wind speed. To identify the distribution of LLJs in Northeastern China, the height at which the maximum horizontal wind velocity was recorded as the LLJ's vertical position, and the wind profile at each data grid was identified as an event. According to the distribution of LLJs, further elucidated in section 3.1.1, two high-frequency LLJ regions were captured (indicated by the red and blue boxes in Fig. 1, in the warm and cold seasons, respectively). Based on this, we define the LLJ days according to the following criteria: as long as there is one LLJ within the two regions and on the pressure layer with the highest occurrence rate of LLJs, it will be considered an LLJ day, else it will be considered a non-LLJ day.

2.3. *Harmonic analysis*

A multiple linear superposition method, proposed by Du et al. (2014), was adopted to investigate the statistical significance of the LLJ diurnal cycle. Essentially, this is a mathematical technique used to decompose complex periodic signals into a sum of simpler sinusoidal functions. This method is particularly useful in analyzing cyclical phenomena, such as diurnal cycles or seasonal variations, in various fields like meteorology, oceanography, and other geophysical sciences. The harmonics represent different periodic components or oscillations present in a time series, the 24-hour and 12-hour harmonics are of particular importance in the context of meteorological and climatological studies, as they represent the daily and semi-daily variations in atmospheric processes.

3. LLJ distribution

3.1. *Spatial distribution*

3.1.1. *Horizontal distributions of LLJ occurrences*

The average horizontal distributions of the LLJ occurrence rate in Northeastern China during the warm and cold seasons of 1957 to 2021 are depicted in Fig. 2. In the warm season, a significant incidence of LLJs is observed over relatively flat regions in the central part of Northeastern China, with an occurrence rate exceeding 12% (the red box in Fig. 2a). In the cold season, the leeward slopes of almost all mountain ranges represent relatively high-frequency areas for LLJs; nevertheless, the highest LLJ occurrence was located within a strip along the leeside of the Da Hinggan Ling

Mountains, with the maximum occurrence rate exceeding 28%. Based on this distribution pattern, we can isolate two high-frequency LLJ regions in Northeast China, one during the warm season (Area 1, red box in Fig. 2) and the

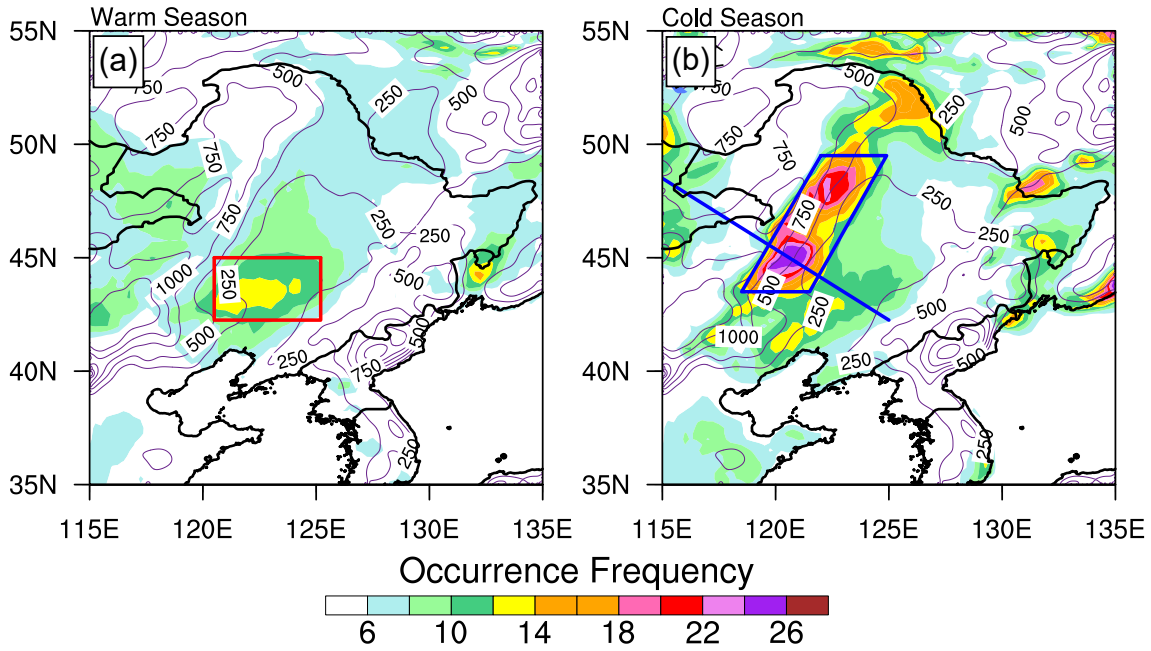

Fig. 2. Horizontal frequency distributions of LLJs (%, shading) during the (a) warm season and (b) cold season in Northeastern China. The dark brown contour lines represent terrain height (m, interval: 250 m). The red and blue boxes indicate the two high-frequency LLJ regions (i.e., Area 1 and Area 2) that are the same as those in Fig. 1.

other during the cold season (Area 2, blue box in Fig. 2).

Regarding wind direction (Fig. 3), LLJs are predominantly southwesterly (including southerly and westerly) in the warm season, with over 50% of the LLJs in this direction. By contrast, during the cold season, the jet direction is predominantly northwesterly (including northerly and westerly), with over 60% of the LLJs in this direction.

3.1.2. *Vertical distribution of LLJ occurrences*

Figure 4 presents the occurrence of LLJs in different layers and vertical profiles of the daily mean wind of LLJs days in the two high-frequency LLJ regions. Analysis reveals that the peak of LLJ occurrence occurs at the 925 hPa in Area 1 during the warm season. In comparison, during the cold season, the layer experiencing the most frequent LLJs in Area 2 is higher, around 875 hPa. By selecting the characteristic pressure level with the most frequent LLJ occurrence in each area, the characteristic pressure levels are determined to be 925 hPa for Area 1 during the warm season and 875 hPa for Area 2 during the cold season. In the following sections, we will focus on these two layers to further explore the characteristics of LLJs in Northeast China.

3.2. *Temporal distribution*

Figure 5 presents the diurnal variations of the occurrence rate of LLJs in Area 1 and Area 2. By fitting the diurnal variations of the LLJ occurrence rate with a multiple linear superposition method (i.e., the two lines in Fig. 5), as described in section 2.3, we measure the goodness of the fit in terms of coefficient of determination [$R^2 = 1 - (\mathrm{SSR}/\mathrm{SST})$], where SSR and SST are the regression and total variance. The contribution of the LLJ rate over a 24-hour to the entire harmonic

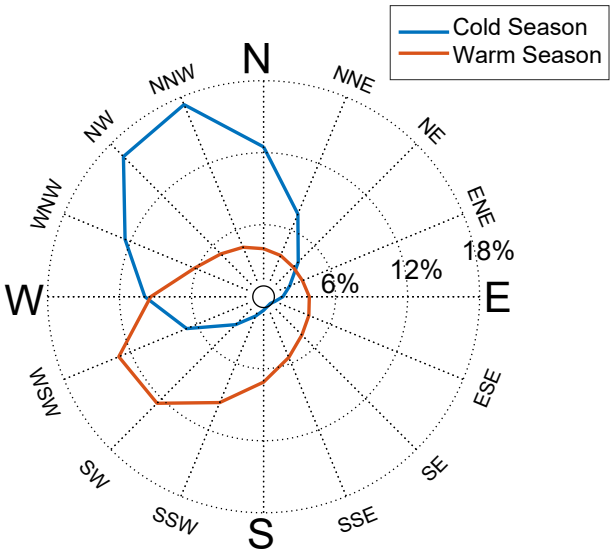

Fig. 3. Wind direction distributions (%) of LLJs over Area 1 during the warm season (orange line) and Area 2 during the cold season (blue line).

pattern exceed 0.95 in both the warm and cold seasons, indicating that LLJs experienced considerable diurnal cycles.

In the warm season, peak LLJ occurrence in Area 1 appeared at midnight at LST (Local Standard Time = UTC + 8 hours), while in the valley, it appeared in the afternoon between 1300 and 1500 LST. In the cold season, the major peak of LLJ occurrence in Area 2 appeared at 2200 LST, which was slightly earlier than in the warm season, while in the valleys, the peak appeared later in the afternoon between 1400 and 1600 LST (Fig. 5). The above conclusions are con-

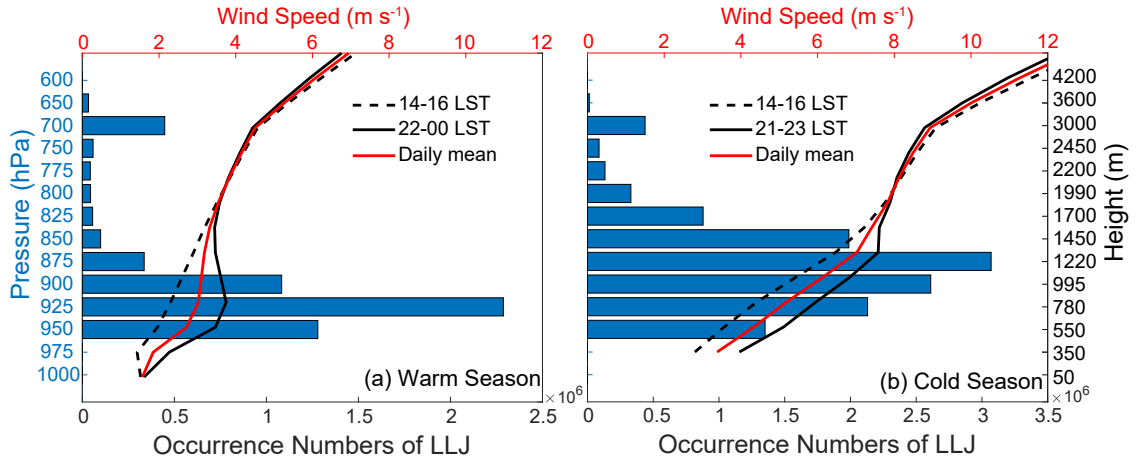

Fig. 4. The number of LLJs at different layers (histogram) and vertical profiles of daily mean wind (m s^{-1}, red lines), 2200–0000 LST and 2100–2300 LST mean wind (m s^{-1}, black solid lines), and 1400–1600 LST mean wind (m s^{-1}, black dashed lines) of LLJ days averaged over (a) Area 1 in the warm season and (b) Area 2 in the cold season.

sistent with previous studies, which show that LLJs primarily occur at midnight and are relatively inactive during the afternoon (Du et al., 2014; Zhang et al., 2018). Interestingly, however, a sub-peak around 1000 LST was found during the cold season. The formation of this sub-peak was found to be a byproduct of the interaction of the flow with the topography, which will be illustrated in section 4.4.

4. Formation and development mechanisms

4.1. *Large-scale environment*

Figures 6a and c compare the large-scale environment of LLJ days between warm and cold seasons. The large-scale forcing over northeastern China is more intense during the cold season, evidenced by the denser isobars and isotherms in Fig. 6c. The high-frequency LLJ region is situated in front of a short-wave trough in the warm season; however, it is located at the rear of a short-wave trough in the cold season. The large-scale circulation between LLJ days (Figs. 6a, c) and non-LLJ days (Figs. 6b, d) are also compared. For both seasons, the large-scale forcing on LLJ days is more intense than that on non-LLJ days. As mentioned earlier, the high-frequency LLJ region is in front of a short-wave trough in the warm season; however, the condition is reversed for non-LLJ days. By contrast, the distinction of circulation patterns between LLJ and non-LLJ days becomes less pronounced for the cold season, indicating a more subtle influence of atmospheric circulation patterns on LLJ formation during this period.

The distinct circulation patterns result in different background winds on the height of the jet core and, therefore, different behaviors of LLJs between warm and cold seasons. Specifically, the wind direction is primarily westerly to southerly (westerly to northerly) in the warm (cold) season, which primally results in the observed differences in wind direction for LLJs in the two seasons (Fig. 3). The more

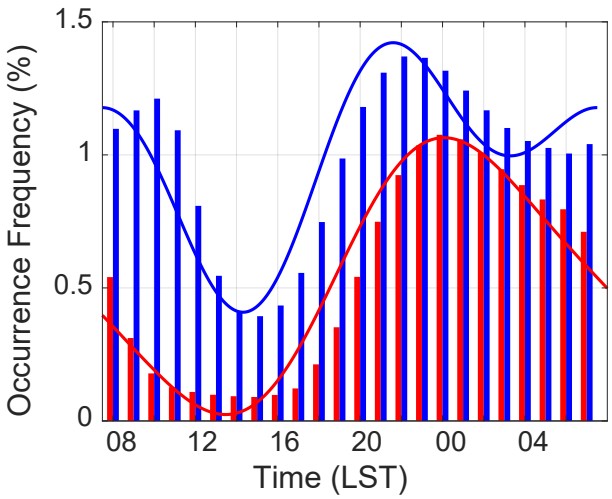

Fig. 5. Diurnal variation of LLJ occurrence frequency during the warm (red) and cold (blue) seasons. Histograms indicate statistical results, while the lines represent fitting results from harmonic analysis.

intense large-scale forcing in the cold season results in more robust low-level winds during that period. In quantitative terms, the mean wind speeds of LLJ days at the core of the LLJs are about 3.6 m s^{-1} in Area 1 during the warm season and 7.7 m s^{-1} in Area 2 during the cold season (red lines in Figs. 4a and b). As a result of the intense background circulation during the cold season, LLJs experience higher wind speeds than their warm season counterparts.

Regulated by the diurnal variation of the large-scale circulations (not shown), the maximum mean wind speed of LLJs at night is greater than that during the day (Fig. 4). The wind speed also increases (decreases) more quickly at night than during the day below (above) the core of the LLJ, visualized in the more nose-like structure of the nighttime wind profiles, especially for LLJs in the warm season. The vertical wind shear is a critical factor in the definition of

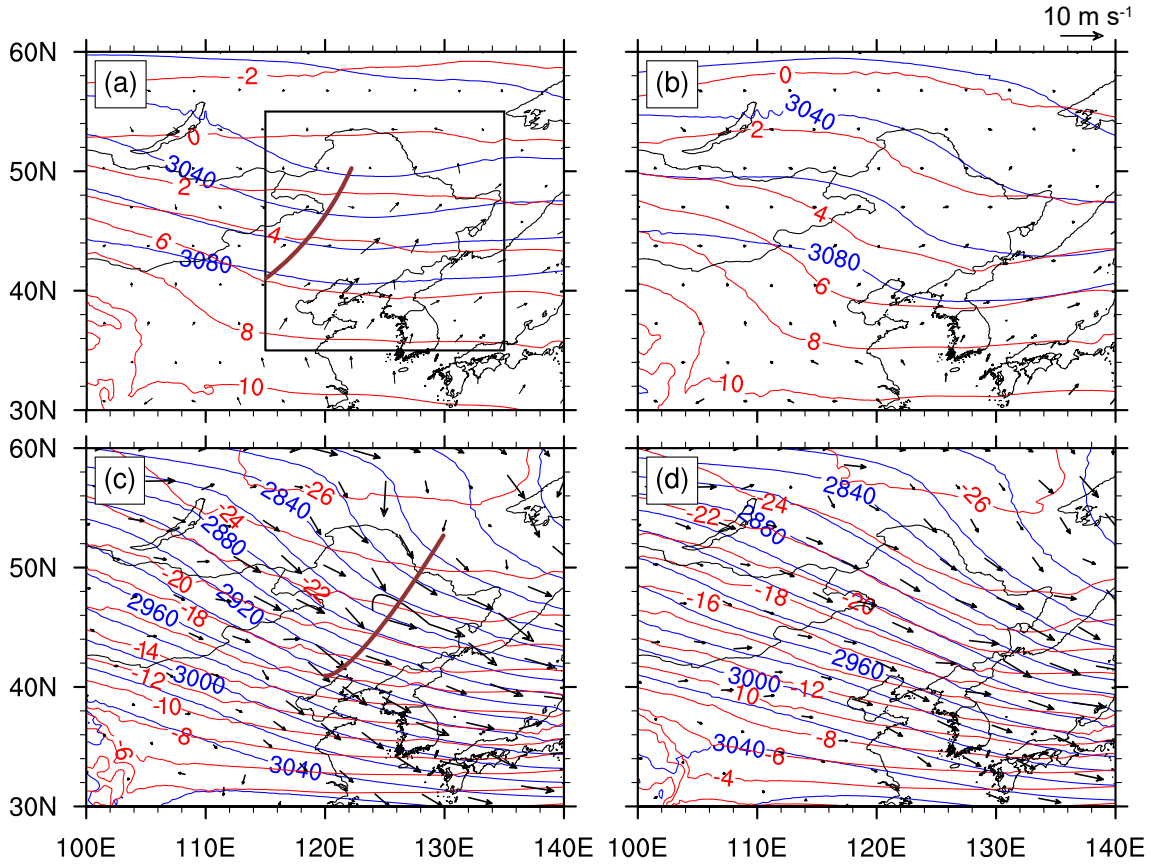

Fig. 6. Comparison of (a, b) warm season and (c, d) cold season 700-hPa geopotential height (m, blue lines) and temperature (°C, red lines), and horizontal winds (m s^{-1}, at 925 hPa for warm seasons and 875 hPa for cold seasons) for (a, c) LLJ days and (b, d) non-LLJ days. The black box indicates the location of Northeast China.

LLJs, and thus, this change in the wind profile is conducive to the formation of the nocturnal LLJ events. The above-mentioned findings highlight the significant effect of large-scale circulation patterns on LLJs over Northeastern China.

4.2. *Topography-flow interaction*

As shown in Fig. 1, Northeastern China is situated within a unique geographical setting, characterized by the presence of mountains on all four sides: the Da Hinggan Ling Mountains lie to the west, the Changbai Mountain Range to the east, the Yanshan Mountain Range to the south, and the Xiao Hinggan Ling Mountains to the north. These mountains jointly regulate the formation and behavior of LLJs in Northeastern China. In the warm season, these mountains collectively create a channeling effect for the southwesterly background winds, as illustrated by the robust southwesterly flow between the Changbai and the Da Hinggan Ling ranges in Fig. 6; thus, they are conducive to the formation of a southwesterly LLJ. In the cold season, the LLJs exhibit more topographic dependency, as indicated by the relatively high concentration of LLJs over almost every eastern slope of these mountain ranges (Fig. 2b). Nevertheless, the eastern slope of the Da Hinggan Ling Mountains experiences the most frequent, as well as the broadest LLJ occurrence. Therefore, in the following subsection, we will discuss exactly how the topography modulates LLJ formation in this region.

To investigate the interaction between the Da Hinggan Ling Mountains and the northwesterly low-level winds, the distribution of the circulation and potential temperature in the cross-section represented by the blue line in Fig. 2 was checked at 2000 LST (i.e., the peak hour of LLJ velocity) during the cold season. In this cross-section, a significant enhancement of the northwesterly winds was captured on the leeside of the Da Hinggan Ling Mountains (Fig. 7). From the view of fluid dynamics, windward steep topography serves as a barrier. The condition that determines whether an air parcel could rise up and over a mountain is determined by the Froude number [Fr, Eq. (1)], a dimensionless parameter that balances the kinetic energy represented by the wind speed (U) against the potential energy represented by the product of the Brunt-Väisälä frequency (N) and the height of the mountain (H_m). If Fr is greater than 1, the flow will pass over the mountain, whereas if it is less than 1, the flow will be blocked by the mountain. When air flows over a mountain, it can be divided into two distinct types: subcritical and supercritical flow (Durran, 1990). Supercritical flow occurs when the flow velocity exceeds the gravity wave speed in the fluid, while subcritical flow occurs when the flow velocity is less than the gravity wave speed, resulting in a low

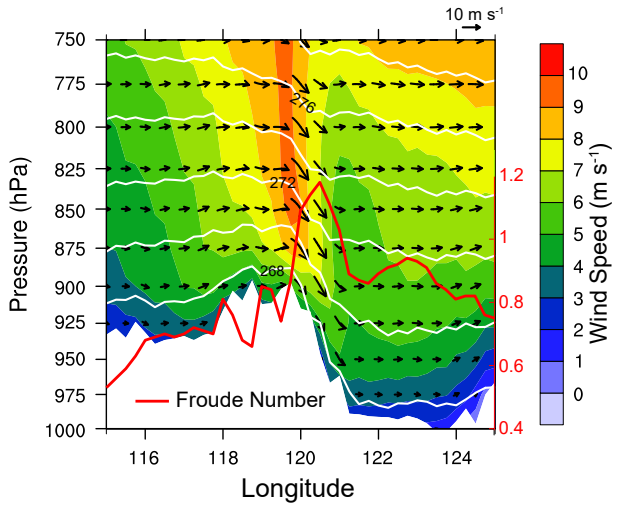

Fig. 7. Vertical circulation (horizontal wind and vertical wind multiplied by 250, m s^{-1}, vectors), wind speed (m s^{-1}, shading), potential temperature (K, white line), and the Froude number at 875 hPa (red line) in the cross-section represented by the blue line in Fig. 2 at 2000 LST during the cold season.

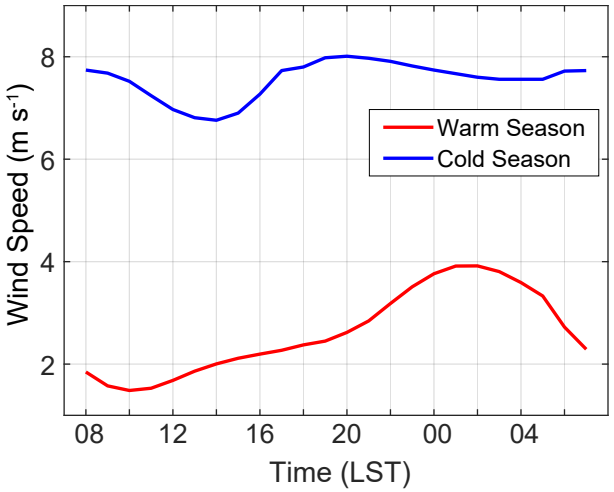

Fig. 8. Variations of the mean wind speed at 925 hPa in Area 1 during the warm season (red line) and at 875 hPa in Area 2 during the cold season (blue line).

Froude number (less than 1).

$$\mathrm{Fr} = \frac{U}{NH_{\mathrm{m}}}. \tag{1}$$

For airflow in the cross-section represented by the blue line in Fig. 2, the red line in Fig. 7 presents how Fr varies with longitude at 875 hPa. The results show that Fr slowly increased but remained less than 1 at times before the mountain but began to exceed 1 after passing the first mountain peak. Upon crossing the second mountain peak, Fr increases rapidly, leading to supercritical flow. Under this condition, the air accelerates as it descends; consequently, leeside enhancement occurs and promotes the formation of an LLJ. As the flow reaches the base of the mountain, it may encounter a sudden change in topography, causing Fr to gradually decrease to below 1, causing the flow to decelerate and transition from supercritical to subcritical flow (Fig. 7). This transition is known as a hydraulic jump (Durran, 1990; Kong et al., 2020), which can be thought of as a sudden rise in fluid height, accompanied by a sharp decrease in the downstream flow velocity. Based on this analysis, the interaction between flow and topography resulted in leeside supercritical flow as well as the narrow strip of high LLJ occurrence over the east slope of the Da Hinggan Ling Mountains during the cold season.

4.3. *Diurnal variations*

As described in section 3.2, both cold-season and warm-season LLJs experience obvious diurnal variations, and, intriguingly, the phases of the two variation patterns are different. To diagnose the underlying cause of the two diurnal variation patterns and their differences, the variation of horizontal wind speed within the two high-frequency LLJ regions is checked (Fig. 8). For the warm season, the horizontal winds are relatively stagnant around 1000 LST; after that, due to the continual acceleration, the wind speed reaches its maximum at 0200 LST and provides a favorable condition for the formation of the peak of LLJ occurrence around 0000 LST (Fig. 5). For the cold season, two wind speed peaks are captured at 0800 and 2000 LST, while the minimum wind speed occurs around 1400 LST. The cold-season wind speed variation corresponds to the double-peak pattern of LLJ occurrence during the same period (Fig. 5).

Notably, the time of maximum LLJ occurrence frequency does not exactly correspond to the time of maximum wind speed (Figs. 5 and 8). This is because both wind speed and wind shear (i.e., the difference between the wind speed of the jet core and the upper and lower layers) are criteria for LLJ identification (as described in section 2.2); further noting that the time it takes for the shear to reach its maximum can modulate the occurrence of the LLJ and account for this time difference. However, how the winds in other layers vary with time is not the subject of this study; hereinafter, from the perspective of different wind components, we will focus on the layer of the LLJ core and explain why the diurnal variation patterns exist.

4.3.1. *Warm season*

As shown in Fig. 9, the wind anomalies at 925 hPa over Area 1 experience a clockwise rotation, which promotes the development of an LLJ between 2200 and 0400 LST when anomalies generally align with the southwesterly background wind. To understand this rotation, we first trace the source of the wind anomalies. From the perspective of topographic thermodynamics, a sloping terrain can alter the horizontal distribution of the surface solar heating rate and the nocturnal cooling rate; therefore, the air temperature at the same altitude is different over higher and lower terrain (Smith, 1979). This inhomogeneity usually leads to mesoscale flows such as slope and valley winds. In northeast China, the atmosphere over mountains warms up faster after sunrise (Figs. 9e–g).

The rapid warming over mountains causes the positive temperature anomalies to be significantly higher than those over the plains. Under this condition, an up-valley wind, which actually causes the wind anomalies, begins to take shape, reaching its peak at 1500 LST. Controlled by this daytime pattern, the wind anomalies in Area 1 are mainly easterlies. However, after sunset, the significant cooling effect over mountains breaks the daytime thermal contrast pattern (Figs. 9a–c); consequently, the valley winds lose the driving force needed to sustain them, thus allowing the wind anomalies start to rotate clockwise under the effect of an inertial oscillation (Fig. 9i). After midnight (Figs. 9b–d), the temperature in northeast China turns into a negative anomaly, which is more pronounced over the mountainous terrain; therefore, the thermal contrast pattern is reversed compared to the afternoon one. In Area 1, the westerly mountain winds take shape and join the clockwise rotation until a new cycle of diurnal variation starts after midday.

$$\underset{\text{TEN}}{\frac{\partial u}{\partial t}} = \underbrace{\left(-u\frac{\partial u}{\partial x} - v\frac{\partial u}{\partial y}\right)}_{\text{ADV}} \underbrace{- w\frac{\partial u}{\partial z}}_{\text{VER}} \underbrace{+ f\left(v - v_g\right)}_{\text{COR}} \underbrace{+ F}_{\text{FRI}} \qquad (2)$$

The qualitative analysis above can be further substanti-

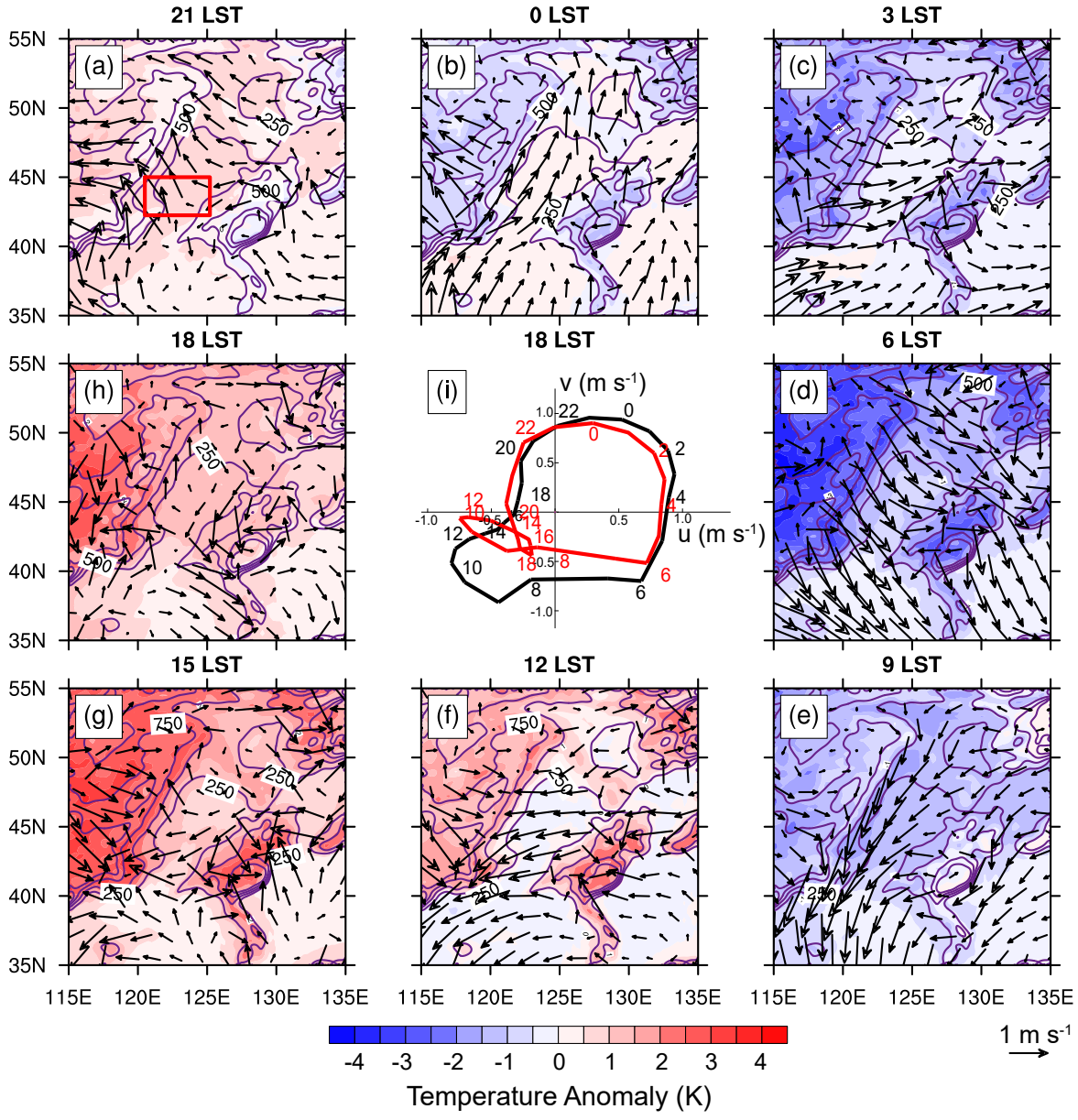

Fig. 9. Diurnal wind anomalies (m s^{-1}, vector) and temperature anomalies (K, shading) at 925 hPa at (a–h) 2100, 0000, 0300, 0600, 0900, 1200, 1500, and 1800 LST during the warm seasons. (i) The black (red) line represents the clockwise rotation of wind anomalies (ageostrophic wind) at 925 hPa (m s^{-1}) averaged in Area 1 [red box in (a)]. The purple contour represents terrain height (m, interval: 250 m).

ated from the perspective of a momentum analysis (Eq. (2)), similar to the approach outlined by Du et al. (2014). It is worth noting that a coordinate transformation was used to visually represent the effects of each term in the momentum budget. Specifically, in Eq. (2), the *x*-direction was aligned with the daily mean wind vector of LLJ days, and the *y*-direction was perpendicular to the *x*-direction and oriented towards the left. The tendency (TEN) term, represented on the left side of the equation, accounted for the local acceleration. The right side of the equation is comprised four terms: the horizontal advection (ADV), vertical advection (VER), Coriolis force acting on the ageostrophic winds in the *x* direction (COR), and residual entities, including but not limited to friction (FRI).

As shown in Fig. 10a, TEN is mainly regulated by COR, indicating that the inertial oscillation of wind anomalies (the ageostrophic wind is roughly equivalent to wind anomalies, Fig. 9i) is the main contributor to the diurnal variation. In accordance with the continuous increase of COR after 0800 LST, TEN becomes positive after 1000 LST, providing a slow acceleration to the atmosphere. After 1800 LST, accompanied by the slight decrease of RES and the continuous enhancement of COR, the magnitude of TEN increases, pointing to a faster acceleration rate in the jet direction. Within this accelerating period, the peak LLJ formed at 0000 LST (Fig. 5). At around 0200 LST, TEN becomes negative, the acceleration effect disappears, and the wind speed in the jet direction starts to decrease. Distinguishable from the traditional inertial oscillation triggered by the sudden decrease of friction after sunset, the magnitude of RES does not change much (Fig. 10a). That is because the trigger here is the break of valley wind in the late afternoon, as described in the first paragraph of this section.

4.3.2. *Cold season*

Similar to the condition in the warm season, wind anomalies at 875 hPa during the cold season are also regulated by the diurnal variation of thermal contrast and experience a clockwise rotation (Fig. 11); and COR is also the main contributor to TEN in the momentum budget (Fig. 10b), indicating that the diurnal variation of wind components is primarily influenced by the veering of wind anomalies. Unlike the slight fluctuation of RES in the warm season (Fig. 10a), the decrease in negative values for RES is considerable after 1400 LST in the cold season (Fig. 10b), which actually helps to increase TEN in the afternoon. This result suggests that a decrease in atmospheric turbulence may also promote the development of an inertial oscillation in the cold season.

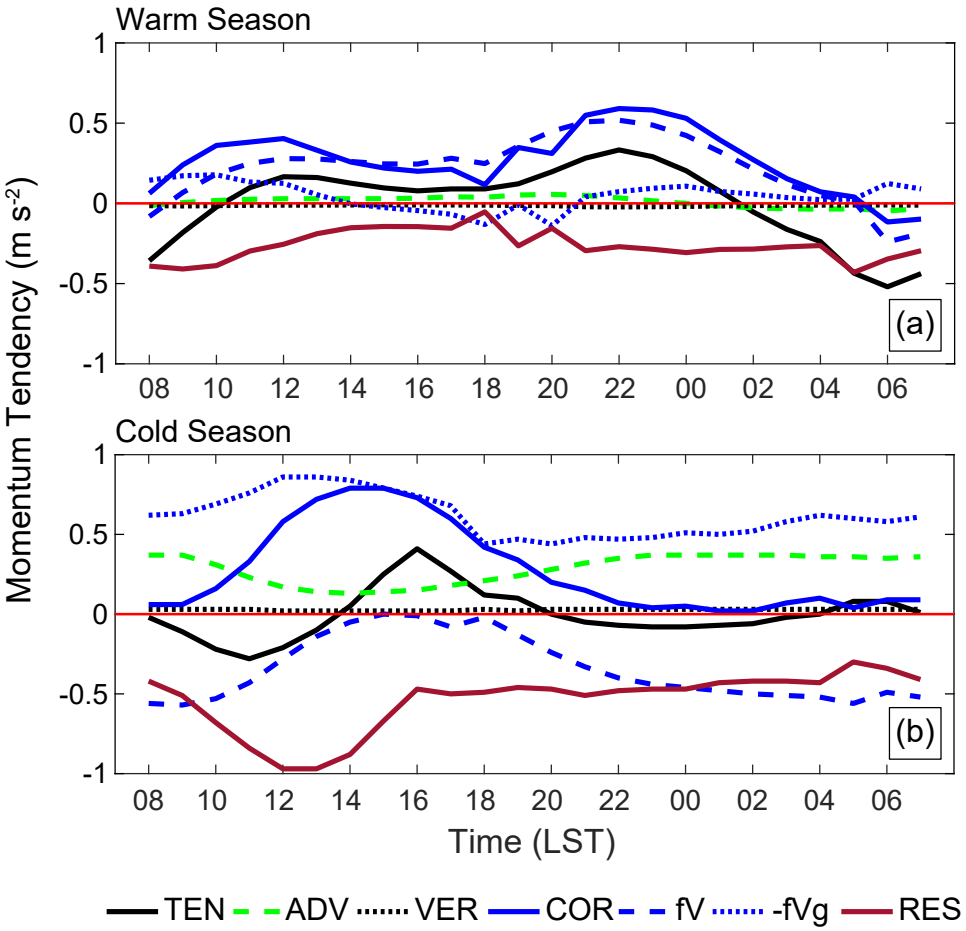

Fig. 10. Diurnal variation of the individual terms in the horizontal momentum equation in the LLJ direction for (a) warm season at 925 hPa in Area 1 and (b) cold season at 875 hPa in Area 2.

Besides, there is still a noticeable difference between the two diurnal variation patterns; that is, the phase of the inertial oscillation in the cold season occurs much earlier than in the warm season (Figs. 9 and 11). The causes of these differences need to be carefully examined.

As previously mentioned, wind anomalies in both seasons are primarily caused by mountain–valley circulations, and the phase of this circulation is roughly determined by the thermal contrast of the temperature anomalies between mountainous and flat regions. Thus, the diurnal variation of this thermal contrast is checked at 925 hPa (875 hPa) in the warm (cold) season (Fig. 12). It is noteworthy that in the ERA5 reanalysis, the peak of the Da Hinggan Ling Mountains (~1230 m) is higher (lower) than that of the layer at 925 hPa (875 hPa). Thus, the east slope (~730 m ASL) and the peak of the Da Hinggan Ling Mountains, indicated by the pink and blue triangles in Fig. 1, respectively, are chosen to represent mountainous regions in the warm season and cold season. Besides, for better comparability between different atmospheric layers, normalization is applied for both seasons (the dashed lines in Fig. 12).

Due to the shorter daylight duration in the cold season (Fig. 12), the positive phase of thermal contrast is shorter and quickly transitions into a negative phase after 1700 LST, three hours earlier than that for the warm season. Consequently, the afternoon wind anomalies (i.e., the valley wind) lose their driving force over a shorter period and enter an inertial oscillation earlier in the cold season. Although the magnitude of the positive thermal contrast in the warm season also decreases after 1200 LST, the long duration of the positive phase coupled with the slow decreasing trend results in a delayed start to inertial oscillation. Besides, the period of inertial oscillations can be calculated using the formula $T = 2\pi/f = \pi/\Omega\sin\varphi$ (Du et al., 2015b). The average latitude for

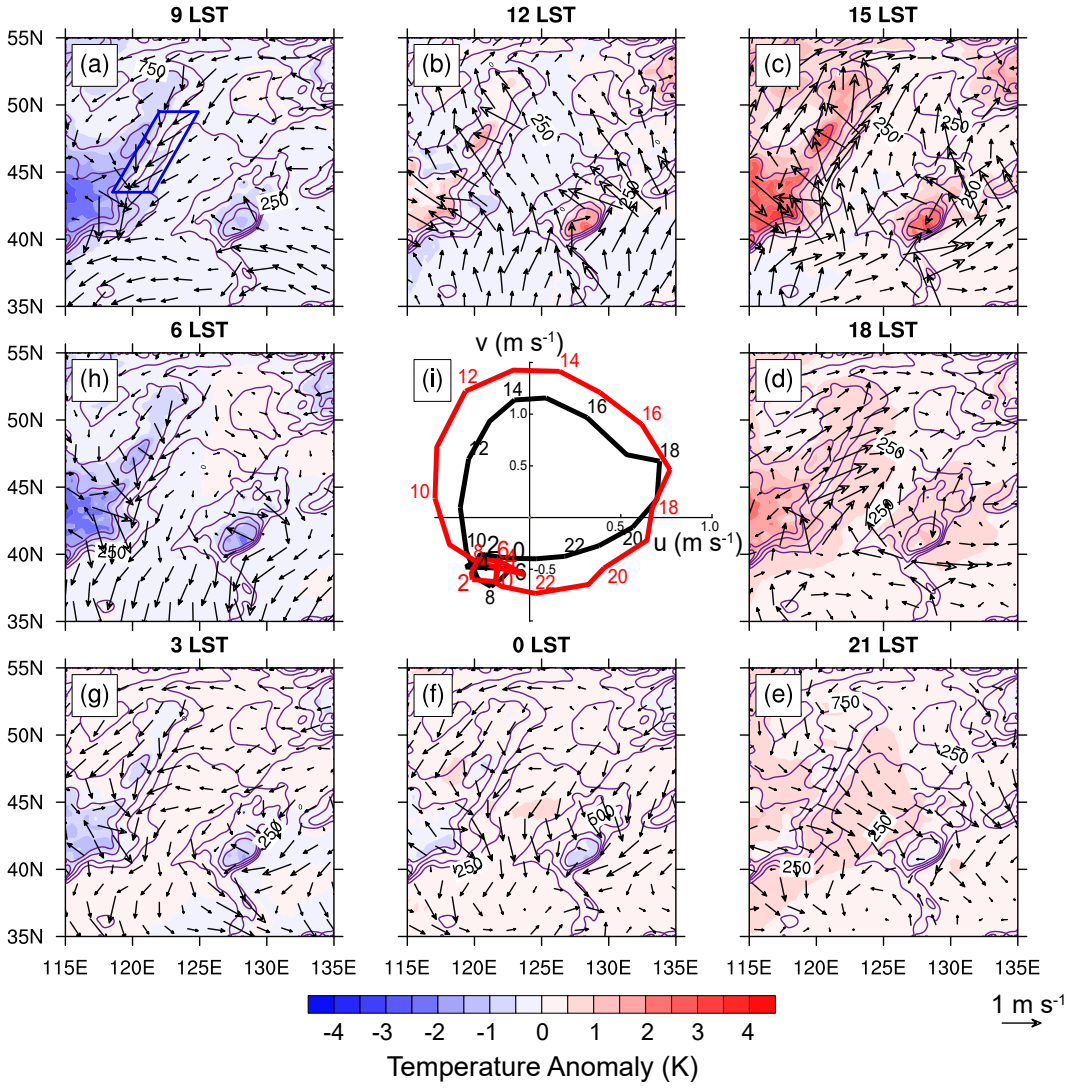

Fig. 11. Diurnal wind anomalies (m s^{-1}, vector) and temperature anomalies (K, shading) at 875 hPa at (a–h) 0900, 1200, 1500, 1800, 0000, 0300, 2100, and 0600 LST, respectively, during the cold seasons. (i) The black (red) line shows the clockwise rotation of wind anomalies (ageostrophic wind) at 875 hPa (m s^{-1}) averaged in Area 2 [the blue box in (a)]. The purple contour represents terrain height (m, interval: 250 m).

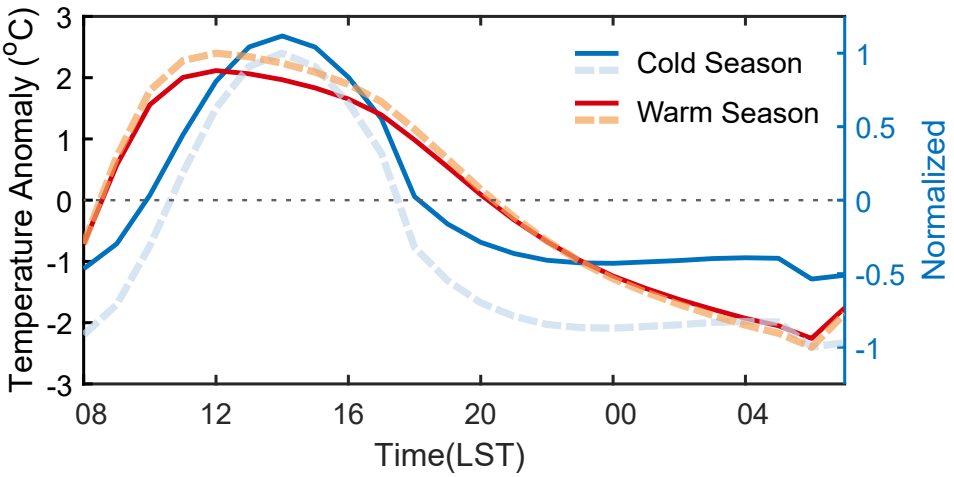

Fig. 12. Diurnal variation of the thermal contrast (°C, the solid lines and left axis) between the atmosphere over the mountainous and foothill regions (triangles and the square in Fig. 1, respectively). The dashed lines (right axis) show the same but for normalized results.

Area 1 in the warm season is 43.75°N, which translates into a period T of approximately 17.5 hours. The ageostrophic wind direction in the warm season begins turning from the southeast at 1800 LST, and after about 7 hours, it turns approximately 190 degrees. Around 0100 LST, the wind direction aligns with the background southwest wind direction (Fig. 9i). By contrast, for Area 2, the average latitude of this region is 47.5°N, making the period of inertial oscillation (about 16.4 hours) shorter than in Area 1. The ageostrophic wind direction starts turning from the southwest wind at 1500 LST, and after about 4 hours, it turns approximately 90 degrees, so by around 2000 LST, the wind direction becomes consistent with the background wind from the northwest (Fig. 11i). In conclusion, the differences in daylight duration, direction of background winds, and latitude of the two high-frequency LLJ regions are considered to be the three main causes for the different phases of inertial oscillation between warm and cold seasons.

4.4. *Sub-peak of the cold-season LLJ*

In the cold season, a sub-peak of LLJ occurrence takes place around 1000 LST, which corresponds to the local maximum of wind speed at 0800 LST (Figs. 5 and 8). As shown in Fig. 13a, the underlying cause of the sub-peak is the intensification of the wind anomalies at 875 hPa, which actually originates at 925 hPa. More specifically, before sunrise, at 925 hPa, high-pressure areas form in mountainous regions due to the lower temperatures over the Da Hinggan Ling Mountains, Yanshan, and Changbai Mountains (Fig. 13b). Consequently, a weak low-pressure anomaly forms in the plains, which drives northeasterlies on its western edge. Meanwhile, northwesterly downslope winds are ongoing. The confluence of these northwesterly downslope winds with the low-pressure-induced northwesterly winds enhances the northerly wind component along the ridge of the Da Hinggan Ling Mountains and, under the influence of fluid viscosity, favors the formation of LLJ at 875 hPa.

This phenomenon also occurs in the warm season (not shown); however, the enhanced northeasterly wind anomaly is nearly in the opposite direction to the southwesterly LLJ. Therefore, it cannot contribute to the formation of LLJs during that period.

5. Conclusion

We employed hourly ERA5 reanalysis data with 25-km horizontal resolution and 14 vertical levels to delve into the formation and development mechanisms of LLJs over Northeastern China during warm and cold seasons from 1957 to 2021. Northeastern China exhibits two high-frequency regions of LLJs: the central region during the warm season and the leeward slopes of the Da Hinggan Ling Mountains during the cold season. The heights, wind characteristics, and diurnal cycles of the LLJs differ in the two regions due to the combined influences of background circulation and terrain. The main findings are summarized as follows:

(1) Warm-season LLJs primarily flow northeastward (Fig. 14a), with the core appearing at 925 hPa, influenced by southwesterly background winds. In comparison, the cold-season LLJs primarily flow southeastward (Fig. 14b), core appearing at 875 hPa. Due to the stronger background winds and terrain-induced supercritical flow, LLJs are more frequent and robust in the cold season.

(2) The inertial oscillation and mountain–valley thermal circulation are the main contributors to the formation and the diurnal variations of LLJs in both seasons (Fig. 14). However, three key differences emerge: a) earlier sunset advances the inertial oscillation in the cold season; b) higher latitudes shorten inertial oscillation periods in the cold season; c) the smaller angle between the background wind and anomalies align faster. These three factors jointly result in distinct oscillation phases, and also different peak hours of LLJ occurrence between the cold and warm seasons.

(3) The uneven temperature distribution of the low-level atmosphere over the complex terrain generates a low

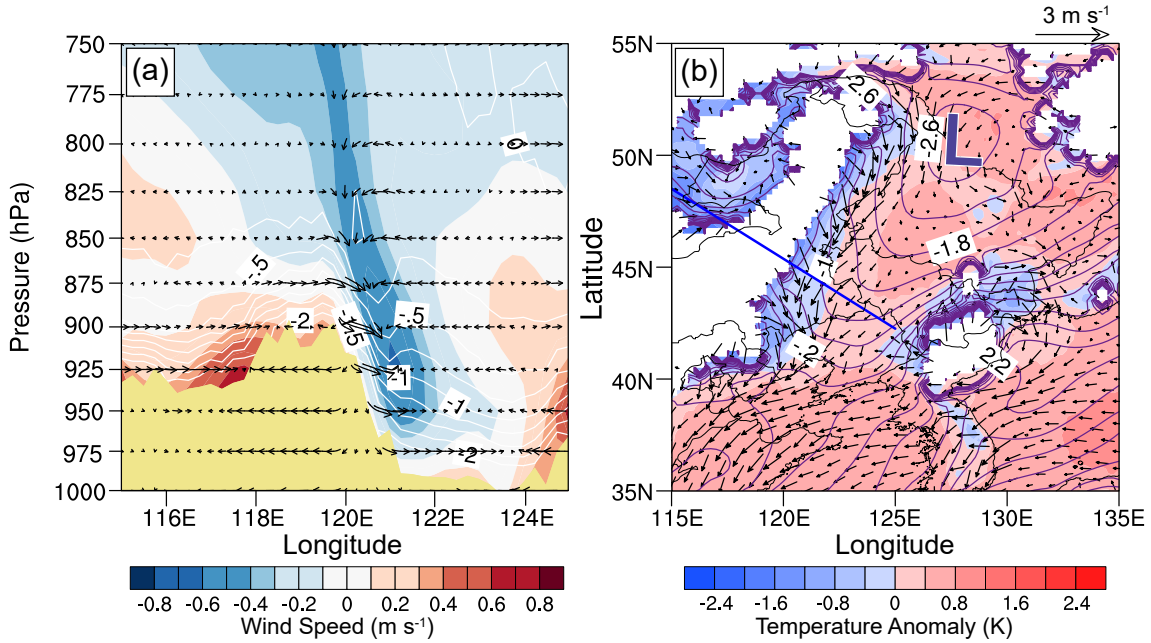

Fig. 13. Temporal circulation anomalies at 0800 LST in the cross-section represented by the blue line in (b) during the cold season. The shading in (a) indicates wind velocity (m s^{-1}) across the cross-section (negative values represent northeasterlies while positive values represent southwesterlies), vectors represent winds (m s^{-1}, horizontal wind and vertical wind multiplied by 5), and lines denote temperature (K); (b) Spatial anomalies of temperature (K, shading), wind (m s^{-1}, vectors), and geopotential height (m, contour) at 925 hPa at 0800 LST. The letter "L" highlights the low pressure over the plain before sunrise.

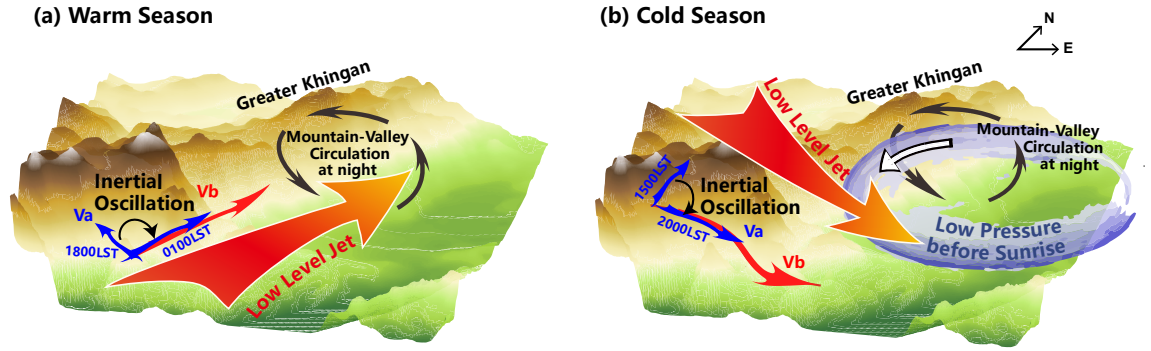

Fig. 14. Schematic of the main processes responsible for the formation of LLJs (red-orange arrows) in Northeastern China during the (a) warm and (b) cold seasons. The black arrows represent the mountain–valley circulation at night; red arrows indicate background wind (Vb); blue arrows indicate the ageostrophic wind (Va) at the starting time of inertial oscillation and the time when Va aligns with Vb; the white arrow in (b) indicates the southward wind anomaly that arises from the low pressure in the valley.

pressure in the valley before sunrise, which results in a southward wind anomaly on the east slope of the Da Hinggan Ling (Fig. 14b). This anomaly is accelerated by the boundary-enhancing effect of the terrain, and under the influence of fluid viscosity, it indirectly leads to the sub-peak of the LLJ at 875 hPa at 0800 LST during the cold season.

This study provides unprecedented insights into spatial and temporal distribution patterns of LLJs over Northeastern China, characterized by intricate terrain and circulation conditions. It examines the formation mechanism of LLJs, potentially applicable to global regions. LLJs play a significant role in shaping local precipitation patterns by enhancing moisture transport and convective activity. Upcoming research endeavors will aim to decipher the specific mechanisms through which LLJs influence precipitation events, thereby advancing our understanding and predictive capabilities regarding regional weather dynamics.

Acknowledgements. This study was supported by the National Natural Science Foundation of China (Grant Nos. 42122033, 42205005, 42075006, and 42475002), the Basic Research and Operation Funding of the Chinese Academy of Meteorological Sciences

(Grant No. 2022Y009), the Key Innovation Team of China Meteorological Administration (CMA2023ZD08), and the Innovation Group Project of Southern Marine Science and Engineering Guangdong Laboratory (Zhuhai) (Grant No. 316323005).

REFERENCES

Blackadar, A. K., 1957: Boundary layer wind maxima and their significance for the growth of nocturnal inversions. *Bull. Amer. Meteor. Soc.*, **38**, 283–290, https://doi.org/10.1175/1520-0477-38.5.283.

Bonner, W. D., 1968: Climatology of the low level jet. *Mon. Wea. Rev.*, **96**, 833–850, https://doi.org/10.1175/1520-0493(1968)096<0833:COTLLJ>2.0.CO;2.

Du, Y., Y.-L. Chen, and Q. H. Zhang, 2015a: Numerical simulations of the boundary layer jet off the southeastern coast of China. *Mon. Wea. Rev.*, **143**, 1212–1231, https://doi.org/10.1175/MWR-D-14-00348.1.

Du, Y., and G. Chen, 2019: Heavy Rainfall Associated with Double Low-Level Jets over Southern China. Part II: Convection Initiation. *Mon. Wea. Rev.*, **147**, 543–565, https://doi.org/10.1175/MWR-D-18-0102.1.

Du, Y., and R. Rotunno, 2014: A Simple Analytical Model of the Nocturnal Low-Level Jet over the Great Plains of the United States. *J. Atmos. Sci.*, **71**, 3674–3683, https://doi.org/10.1175/JAS-D-14-0060.1.

Du, Y., R. Rotunno, and Q. H. Zhang, 2015b: Analysis of WRF-simulated diurnal boundary layer winds in eastern China using a simple 1D model. *J. Atmos. Sci.*, **72**, 714–727, https://doi.org/10.1175/JAS-D-14-0186.1.

Du, Y., Y. A. Shen, and G. X. Chen, 2022: Influence of coastal marine boundary layer jets on rainfall in South China. *Adv. Atmos. Sci.*, **39**, 782–801, https://doi.org/10.1007/s00376-021-1195-7.

Du, Y., Q. H. Zhang, Y. Ying, and Y. M. Yang, 2012: Characteristics of low-level jets in Shanghai during the 2008–2009 warm seasons as inferred from wind profiler radar data. *J. Meteor. Soc. Japan*, **90**, 891–903, https://doi.org/10.2151/jmsj.2012-603.

Du, Y., Q. H. Zhang, Y.-L. Chen, Y. Y. Zhao, and X. Wang, 2014: Numerical simulations of spatial distributions and diurnal variations of low-level jets in China during early summer. *J. Climate*, **27**, 5747–5767, https://doi.org/10.1175/JCLI-D-13-00571.1.

Durran, D. R., 1990: Mountain waves and downslope winds. *Atmospheric Processes over Complex Terrain*, R. M. Banta et al., Eds., American Meteorological Society, 59–81, https://doi.org/10.1007/978-1-935704-25-6_4.

Ferguson, C. R., 2022: Changes in great plains low‐level jet structure and associated precipitation over the 20th century. *J. Geophys. Res.: Atmos.*, **127**, e2021JD035859, https://doi.org/10.1029/2021JD035859.

Fritsch, J. M., R. J. Kane, and C. R. Chelius, 1986: The contribution of mesoscale convective weather systems to the warm-season precipitation in the United States. *J. Climate Appl. Meteorol.*, **25**, 1333–1345, https://doi.org/10.1175/1520-0450(1986)025<1333:TCOMCW>2.0.CO;2.

Hoecker, W. H., 1963: Three southerly low-level jet systems delineated by the weather bureau special Pibal network of 1961. *Mon. Wea. Rev.*, **91**, 573–582, https://doi.org/10.1175/1520-0493(1963)091<0573:TSLJSD>2.3.CO;2.

Holton, J. R., 1967: The diurnal boundary layer wind oscillation above sloping terrain. *Tellus*, **19**, 199–205, https://doi.org/10.1111/j.2153-3490.1967.tb01473.x.

Hsueh, Y., 1970: A note on the boundary layer wind structure above sloping terrain. *J. Atmos. Sci.*, **27**, 322–327, https://doi.org/10.1175/1520-0469(1970)027<0322:ANOTBL>2.0.CO;2.

Jiménez-Siménez, G., P. M. Markowski, G. S. Young, and D. J. Stensrud, 2020: The Orinoco low‐level jet: An investigation of its mechanisms of formation using the WRF model. *J. Geophys. Res.: Atmos.*, **125**, e2020JD032810, https://doi.org/10.1029/2020JD032810.

Kong, H., Q. H. Zhang, Y. Du, and F. Zhang, 2020: Characteristics of coastal low‐level jets over Beibu gulf, China, during the early warm season. *J. Geophys. Res.: Atmos.*, **125**, e2019JD031918, https://doi.org/10.1029/2019JD031918.

Li, J., and Y.-L. Chen, 1998: Barrier jets during TAMEX. *Mon. Wea. Rev.*, **126**, 959–971, https://doi.org/10.1175/1520-0493(1998)126<0959:BJDT>2.0.CO;2.

Lima, D. C. A., P. M. M. Soares, A. Semedo, and R. M. Cardoso, 2018: A global view of coastal low-level wind jets using an ensemble of reanalyses. *J. Climate*, **31**, 1525–1546, https://doi.org/10.1175/JCLI-D-17-0395.1.

Liu, H. B., M. Y. He, B. Wang, and Q. H. Zhang, 2014: Advances in low-level jet research and future prospects. *Acta Meteorologica Sinica*, **28**, 57–75, https://doi.org/10.1007/s13351-014-3166-8.

Liu, X. Y., G. X. Chen, S. J. Zhang, and Y. Du, 2023: Formation of low-level jets over southern China in the Mei-Yu season. *Adv. Atmos. Sci.*, **40**, 1731–1748, https://doi.org/10.1007/s00376-023-2358-5.

Luo, Y. H., and Y. Du, 2023: The roles of low-level jets in "21·7" Henan extremely persistent heavy rainfall event. *Adv. Atmos. Sci.*, **40**, 350–373, https://doi.org/10.1007/s00376-022-2026-1.

Maddox, R. A., 1983: Large-scale meteorological conditions associated with midlatitude, mesoscale convective complexes. *Mon. Wea. Rev.*, **111**, 1475–1493, https://doi.org/10.1175/1520-0493(1983)111<1475:LSMCAW>2.0.CO;2.

Muñoz, E., A. J. Busalacchi, S. Nigam, and A. Ruiz-Barradas, 2008: Winter and summer structure of the Caribbean low-level jet. *J. Climate*, **21**, 1260–1276, https://doi.org/10.1175/2007JCLI1855.1.

Rife, D. L., J. O. Pinto, A. J. Monaghan, C. A. Davis, and J. R. Hannan, 2010: Global distribution and characteristics of diurnally varying low-level jets. *J. Climate*, **23**, 5041–5064, https://doi.org/10.1175/2010JCLI3514.1.

Smith, R. B., 1979: The influence of mountains on the atmosphere. *Advances in Geophysics*, **21**, 87–230, https://doi.org/10.1016/S0065-2687(08)60262-9.

Song, J., K. Liao, R. L. Coulter, and B. M. Lesht, 2005: Climatology of the low-level jet at the southern great plains atmospheric boundary layer experiments site. *J. Appl. Meteorol.*, **44**, 1593–1606, https://doi.org/10.1175/JAM2294.1.

Wang, D. Q., Y. C. Zhang, and A. N. Huang, 2013: Climatic features of the south-westerly low-level jet over southeast China and its association with precipitation over East China.

Asia-Pacific Journal of Atmospheric Sciences, **49**, 259–270, https://doi.org/10.1007/s13143-013-0025-y.

Wei, W., H. S. Zhang, and X. X. Ye, 2014: Comparison of low‐level jets along the north coast of China in summer. *J. Geophys. Res.: Atmos.*, **119**, 9692–9706, https://doi.org/10.1002/2014JD021476.

Wexler, H., 1961: A boundary layer interpretation of the low-level jet. *Tellus A*, **13**, 368–378, https://doi.org/10.3402/tellusa.v13i3.9513.

Whiteman, C. D., X. D. Bian, and S. Y. Zhong, 1997: Low-level jet climatology from enhanced rawinsonde observations at a site in the southern great plains. *J. Appl. Meteorol.*, **36**, 1363–1376, https://doi.org/10.1175/1520-0450(1997)036<1363:LLJCFE>2.0.CO;2.

Zhang, F., Q. H. Zhang, Y. Du, and H. Kong, 2018: Characteristics of coastal low‐level jets in the Bohai Sea, China, during the early warm season. *J. Geophys. Res.: Atmos.*, **123**, 13 763–13 774, https://doi.org/10.1029/2018JD029242.